Combust. Sci. and Tech., 177: 1339–1364, 2005

ISSN: 0010-2202 print/1563-521X online
DOI: 10.1080/00102200590950502

Taylor & Francis
Taylor & Francis Group

SIDE AIR-JET MODULATION FOR CONTROL OF HEAT RELEASE AND PATTERN FACTOR

O.TUNCER
S. ACHARYA*

Department of Mechanical Engineering, Louisiana State University, Baton Rouge, Louisiana, USA

J. COHEN
A. BANASZUK

United Technologies Research Center, East Hartford, Connecticut, USA

The effect of a forced dilution air jet, introduced through the combustor shell, on the air/fuel mixing in the combustion chamber has been investigated. Thermocouple-based temperature measurements have been made at a number of forcing frequencies in the range 100–1100 Hz and blowing ratios in the range 10–15. Open-loop integral flame response to forcing has also been acquired by recording pressure and heat release spectra. A CH-radical imaging technique is used to provide spatially and temporally resolved information about the heat release behavior. The results exhibit that the mean temperature field inside the main reaction zone can be significantly

Received 21 March 2003; accepted 7 December 2004.

This work was supported by a grant from the Office of Naval Research Propulsion Program with Dr. Gabriel Roys as the program monitor. This support is gratefully acknowledged. The help and support received from Dr. Jong-Ho Uhm in doing the CH-imaging measurements is sincerely appreciated. The help and support received from Mr. Yap-Sheng Goh in the various facets of the work is also acknowledged. Helpful discussions with Dr. Satish Narayanan from United Technologies Research Center UTRC and Dr. Jeff Lovett from Pratt & Whitney are also acknowledged. Support to (UTRC) was provided by AFOSR grants F49620-98-C-0006 and F49620-01-C-0021.

*Address correspondence to acharya@me.lsu.edu

altered as a consequence of air-jet modulation. The most significant effects are observed by forcing at vertical locations that are close to the dump plane. Enhancements in temperature of the order of 100–200°C and reduction in pattern factor of the order of 40% were observed, with the lowest pattern factors achieved at the lowest forcing frequency of 100 Hz.

Keywords: spray combustion, mixing, forced dilution jet

INTRODUCTION

Key performance metrics for gas-turbine combustors and propulsion systems include volumetric heat release, pattern factor (PF) and emissions. These metrics are controlled primarily by the combustor stochiometry and the degree of fuel/air mixing. In a typical nonpremixed combustor, both fuel and combustion air are introduced longitudinally at the dump plane, and swirl is generally utilized to mix the fuel and air streams together. In certain combustor designs, additional primary and dilution air are introduced radially through circumferential holes located along the combustor shell. These air jets in crossflow not only provide the air needed to control the stochiometry but also generate enhanced fuel/air mixing. Therefore, the proper design and utilization of these air jets can provide a means toward controlling the fuel/air mixing and enhancing the performance metrics. Increased mixedness, for example, can provide lower pattern factor, lower emissions, and higher volumetric heat release.

Numerous experimental and numerical studies have been carried out on the structure of turbulent transverse jets and have shown that the entrainment and mixing processes can be enhanced by modulating the jet flow (Blossey et al., 2001; Cho et al., 1998; Cortolezzi and Karagozian 2001; Johari et al., 1999; Karagozian et al., 2002; Narayanan et al. 2002; Vermeulen and Yu, 1985; Vermeulen et al., 1982, 1986). These studies suggest that the enhanced entrainment is mainly due to the structural formation of counter-rotating vortex pairs (Cortolezzi and Karagozian, 2001) and/or due to toroidal vortices, which are formed close to the jet exit (Vermeulen and Yu, 1985). For high blowing ratios, wake vortices behind the jet are also observed (Narayanan et al., 2002). Acoustic forcing is found to trigger certain modes of these vortex instabilities that have Lagrangian dynamics (Cortolezzi and Karagozian, 2001). There is a general agreement in the literature that the open-loop jet response is

optimized at the preferred mode jet frequencies that correspond to Strouhal numbers in the range of $0.1 < Sr < 0.3$ (Blossey et al., 2001; Narayanan et al., 2002; Vermeulen and Yu, 1985; Vermeulen et al., 1986). Enhanced vortex dynamics and entrainment of the crossflow leads to increased molecular mixing between the air and fuel species that, in turn, control the combustion processes and the heat release. Because the heat release influences the temperature, the measured temperature distribution inside the combustion chamber can be used to quantify the enhanced entrainment and mixing processes in the combustor.

Numerous researchers have carried out mixing studies of multiple cold-air jets injected into a subsonic isothermal hot crossflow in cylindrical conduits. One such study is due to Holdeman et al. (1996), where an exhaustive search in the parameter space (number of jets, momentum flux ratio, jet-to-total mass flow ratio, jet spacing, density ratio, etc.) was done numerically to obtain an empirical self-similarity parameter denoted as C (known as the Holdeman parameter). Lilley (2002) experimentally investigated an isothermal round jet injected into a swirling crossflow in the absence of combustion.

Vermeulen et al. (1982), in their pioneering effort, attempted to modify the exit-plane temperature distribution of a combustor by acoustically modulating the dilution air-jet streams located close to the exit plane. A difference in temperature of the order of 10°C was observed with modulation due to increased jet mixedness. Furthermore, the uniformity in the temperature distributions appeared to be influenced favorably by the modulation. Crocker et al. (1994) operated an Allied Signal Engines' F-109 combustor at sea level takeoff conditions and reduced the baseline pattern factor by changing the injection angle of dilution air jets. They reported a best-case pattern factor reduction from 0.163 to 0.102 (37% decrease). Such passive control techniques commonly find use in the gas-turbine industry to reduce the baseline PF around nominal operating conditions for increased engine life and greater thrust. Active control through forcing of side air jets holds promise for further PF reduction from the baseline condition. Furthermore, when forcing is controlled with a feedback control algorithm, achievement of minimal possible PFs at a multitude of load conditions can be possible. This is an intrinsic advantage for active control with side air jet injection because passive design techniques can neither adapt to changes in load conditions nor adapt to slow changes in system parameters due to aging. On the other hand, an adaptive control algorithm would simply select

the right forcing frequency to reduce the PF to address off-design changes in flow conditions or changes in geometry with aging.

The goal of the present experimental study is to manipulate fuel/air mixing in a swirl-stabilized spray combustor through modulation of the side air jets and to examine the impact of this manipulation on the PF and volumetric heat release. It is expected that modulation of the air jets will provide improved fuel/air mixing, and that the greatest impact will be achieved at a specific frequency. As pointed out by Holdeman et al. (1996) and Holdeman (1993), the goal of an improved design should not only be to reduce the PF to its lowest value, but to achieve this over the shortest possible distance.

As noted earlier, greater uniformity in the temperature distribution or lower PF is important for a variety of reasons: (1) thermal gradients and stresses acting on the turbine blades can be reduced, thereby extending blade life; (2) NO_x emissions are likely to be reduced by eliminating hot spots; and (3) volumetric heat release in the main reaction zone is enhanced by increasing the temperatures in the cold-spot regions near the endwalls, and between the injectors. Furthermore, improved fuel/air mixing at a shortest possible height enables the design of compact propulsion systems.

EXPERIMENTAL APPARATUS

A schematic of the experimental setup showing all major components is presented in Figure 1. The combustor shell is cylindrical with a diameter (D) of 193.7 mm and a height (H) of 762 mm. Ethanol (C_2H_5OH) fuel is injected at the center through a Parker-Hannifin research simplex atomizing nozzle, which has an approximate spray cone angle of 26°. A 45° swirl vane with a 5-mm exit diameter through which atomization air is delivered surrounds the nozzle tip. Main combustion air is fed through a 45° swirl vane with inner and outer diameters of 34 and 63 mm, respectively (see Figure 2). Using the correlation suggested by Beer and Chigier (1972), the corresponding swirl number is calculated to be $Sw = 0.73$. Hence, swirl inside the combustion chamber is of moderate intensity and generically represents the flow structure inside many of the commercially available gas-turbine combustors. The step height at the dump plane is nearly 65 mm. A 38×64 mm quartz window mounted on the shell enables optical access for CH imaging and photodiode measurements. A number of thermocouple ports are located at different elevations and angular locations, and B-type thermocouples are used

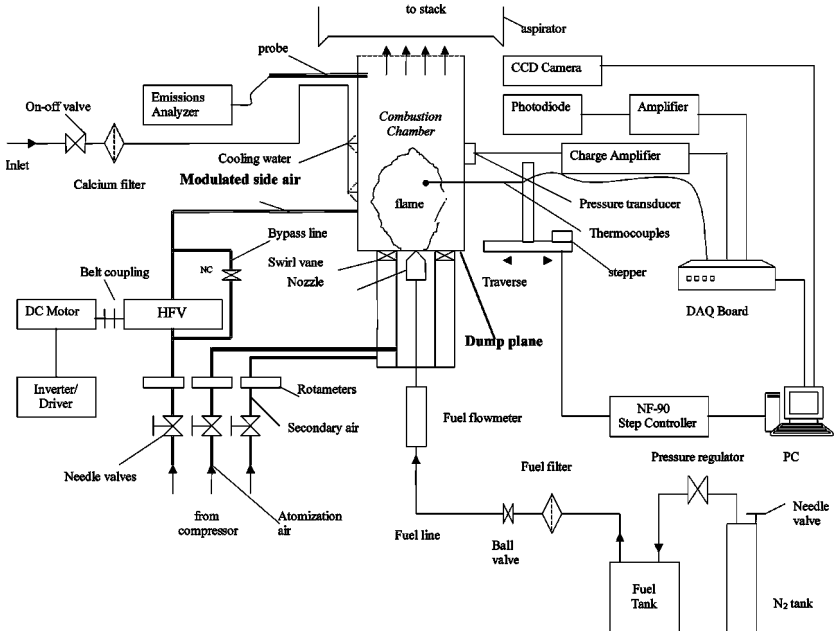

Figure 1. Schematic layout of the experimental setup.

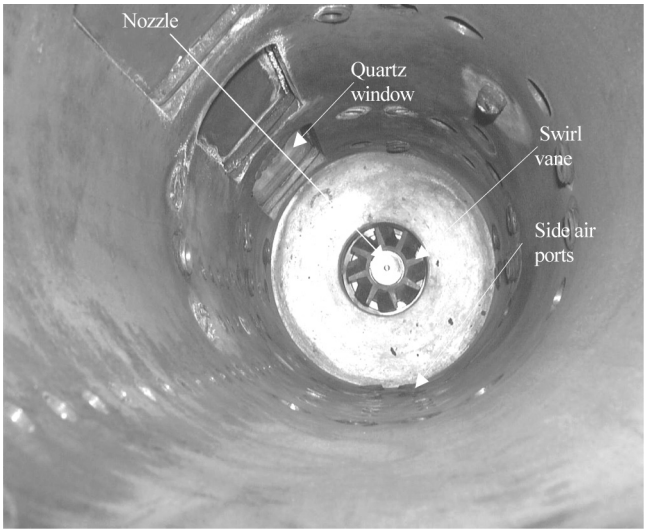

Figure 2. Inside view of the combustion chamber.

to map the temperature distribution inside the combustor. Typically, a rake with four thermocouples mounted on an automated traverse is used for obtaining the temperature distributions inside the combustor.

Fuel is delivered to the combustor through a tank pressurized by compressed nitrogen. A dual-gauge pressure regulator controls the upstream pressure of the nitrogen gas to achieve the desired fuel flow rate. The air needed for atomization, for primary combustion, and for the side air jets is delivered through independent compressed air lines each controlled by individual pressure regulators and needle valves. These compressed air lines, feed off large storage tanks fed by a 290 psig, 450ACFM Atlas-Copco air compressor.

Injection holes for side air jets, each 9.5 mm in diameter and uniformly distributed in the circumferential direction, are located at several elevations along the combustor height (see Figure 2). In this study, four injection holes ($n = 4$) located at an elevation z/D of 0.2 and circumferential spacing S/D of 0.56 [where S is defined as per Holdeman (1993)] are chosen to modulate the main reaction zone. The circumferential locations of the four injection holes are shown in Figure 3, and are chosen such that they have a certain offset ($a/D = 0.16$) with respect to each other. This offset magnitude was chosen arbitrarily, and no optimization of this offset has been attempted in this paper. The offset direction is such that the injected air assists the swirling motion of the main combustion air and can provide varying degrees of swirl depending on the momentum ratio of the injected air.

Modulation of the side air is accomplished by routing it via a spinning valve that has a hollow disk with 20 holes drilled at its periphery, rotating inside a stationary housing that has two discharge holes (O'Donnell, 2001). As the spinner element rotates, stationary and moving holes match at a frequency governed by the rotational speed of the spinner element. A representative time history of jet exit velocity measured by a hot-wire anemometer is shown in Figure 4. The air-jet velocity varies around a mean value at a frequency dictated by the rotational speed of the spinner element. Velocity output is not a pure sinusoid due to the nonnegligible contributions from the harmonic components, which arise from the nonlinearities in the system; yet the output is periodic, as evidenced by the three full cycles shown in Figure 4.

The magnitude of the velocity modulations is proportional to the airflow rate and the frequency of the spinning valve. The frequency response of the spinning valve in the range 50–1000 Hz (approximate range of interest to the present study) is shown in Figure 5 and does

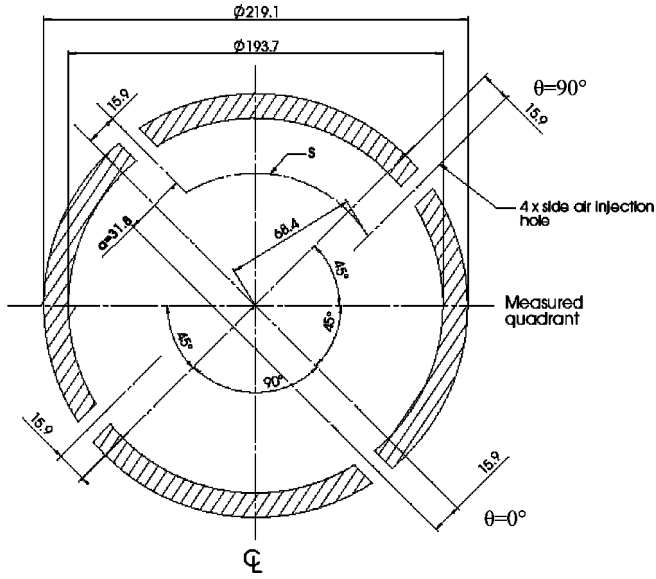

Figure 3. Section view of the combustor at $z/D = 0.2$ depicting the side air injection holes (all dimensions in mm).

not show a perfectly flat response. Rather, the response is somewhat uneven due to the acoustic eigenfrequencies of the spinning valve with variations in the range 74–86 dB. At higher frequencies, the response

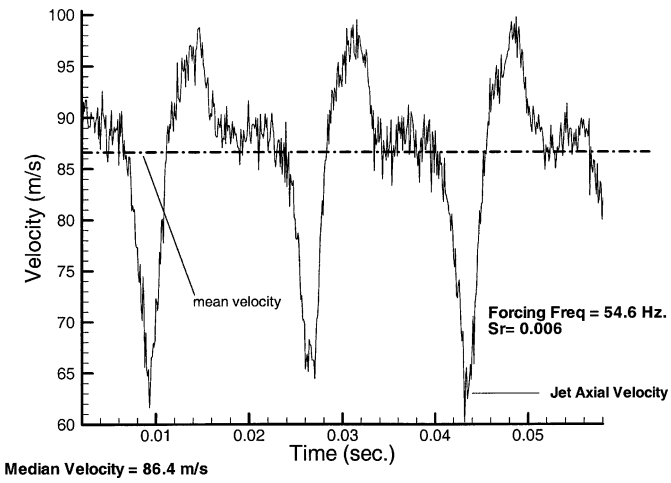

Figure 4. Time history of jet exit velocity ($R = 15$).

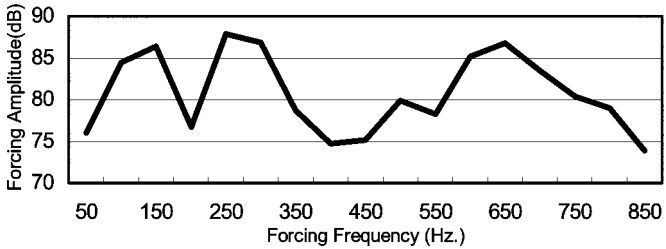

Figure 5. Frequency response of the spinning valve ($R = 15$).

drops off, and if the frequency response were to be plotted over a broad range of frequencies (e.g., up to 100 kHz) on a logarithmic scale, it would show a relatively flat region (variations of the order shown in Figure 5) in the lower frequency range of interest, followed by a rapid decay at higher frequencies. Since it was anticipated from the literature that the side air jet would be most responsive for modulation in the Strouhal number range 0.1–0.4, only the lower frequency range ($Sr < 0.4$, $f < 1.5$ kHz) is of interest to the present study, and the frequency response is examined only in this region. Because both forcing frequency and forcing amplitude are important parameters, frequencies are chosen in the 100–1100 Hz range since they correspond to Strouhal numbers in the range 0.03–0.3, and the modulation amplitude is roughly the same over this range (Figure 5). The selected frequencies are 100, 300, 450, 600, 850, and 1100 Hz, and, as seen in Figure 6, the maximum amplitude variation in this range is about 4 dB. Experiments were also conducted with loudspeakers as actuators (to adjust the amplitude freely), instead of high frequency valve (HFV), and these have shown that a 4-dB range of amplitude variation maintains the temperature readings within uncertainty levels. Therefore, one can be reasonably confident that the amplitude effects are completely factored out.

The fuel and airflow rates are obtained by a series of rotameters and pressure gauges. The measurement accuracy of the air and fuel flow rates are $\pm 2.0\%$ and the measurement accuracy for the pressure gauges mounted at the exit of airflow meters are $\pm 1.0\%$. This yields an overall measurement accuracy of $\pm 4.5\%$ in the equivalence ratio.

Temperature is measured by B-type Pt–Ro thermocouples. Each set of temperature data is obtained using a thermocouple rake that is inserted inside the reacting flow and than traversed radially outward with a VELMEX-1500 series X-Z traverse controlled by an NF-90 stepper-motor controller and a personal computer. Temperature readings are

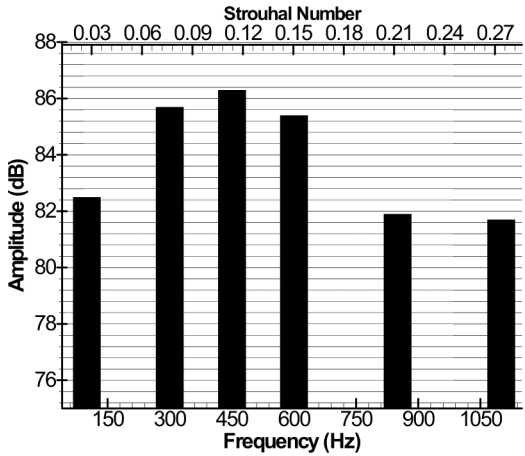

Figure 6. Relative forcing amplitude with respect to forcing frequency ($R = 15$).

averaged over a time period of 30 with 2000 samples collected at each point to ensure that no averaging errors are introduced. Thermocouple readings are corrected for radiation losses. Overall repeatability of the temperature measurements is determined to be ± 20 K.

Pressure variations in the combustor and heat release from the flame are also measured. The integral heat release is arbitrarily quantified with a photodiode looking at the flame. An optical CH filter mounted on the photodiode allows the light at $\lambda = 390$ nm, corresponding to the CH radical emission, to pass through and attenuate all other wavelength contributions. Although there is no strict linear relation between CH intensity and heat release, for ethanol flames, CH intensity has been shown to monotonically increase with heat release (Bertran et al., 1998). A Kistler 7061 water-cooled piezoelectric pressure transducer is mounted along the combustor walls, and measures the pressure inside the combustion chamber. Both heat release (or CH intensity) and pressure spectra are computed with an SRS-785 spectrum analyzer. An intensified CCD camera is used to resolve the temporal and spatial heat release characteristic through cycle-resolved CH-imaging technique.

RESULTS AND DISCUSSION

The combustor is operated close to stochiometric conditions with an overall equivalence ratio (based on total air through the front end and

the side jets) of $\phi = 0.9$. NO_x emissions are particularly high at near-stochiometric conditions (Alder et al., 2000; Roy, 1998), and reduction in PF is likely to help in reducing NO_x. Although the impact of side air-jet modulation on the PF will be explored in the present study, measurements of NO_x have not been undertaken. These measurements are planned for a later phase of the research.

Isothermal crossflow mixing studies (Blossey et al., 2001; Narayanan et al., 2002) show that forcing has a reasonably positive effect for blowing ratios greater than 6 ($R \geq 6$). In the present study with reacting flow, preliminary experiments (with HFV actuation) conducted in the range $6 \leq R < 10$ did not show big differences in the time-averaged temperatures measured at different forcing frequencies. A blowing ratio of 15 resulted in measurable differences and a beneficial impact on PF. Therefore, it can be concluded that at lower blowing ratios the jet is unable to penetrate effectively and/or the modulation does not have sufficient control authority, whereas for higher blowing ratios (e.g., $R = 15$) the penetration is substantial and the modulation influences the temperature distributions substantially. Therefore, data are taken at two distinct blowing ratios, $R = 15$ and 10. The majority of the results are presented for $R = 15$ whereas limited results are presented at $R = 10$ to illustrate the ineffectiveness of control at lower blowing ratios.

The front-end equivalence ratios (based on air delivered only through the front end) are $\phi = 1.7$ and $\phi = 1.4$ for $R = 15$ and $R = 10$, respectively. Global equivalence ratio (based on total air) is held constant at 0.9 during modulation of the side air jets. As noted earlier, the side air jet is modulated at six different frequencies (100, 300, 450, 600, 850, and 1100 Hz) with comparable excitation amplitudes (see Figure 6) to allow an unbiased comparison of the effect of the modulation frequencies without influencing this effect by the forcing amplitude. The Strouhal numbers ($Sr = fd/u_{\text{jet}}$, where f denotes the forcing frequency and d is the jet exit diameter) corresponding to the six forcing frequencies are $Sr = 0.026$, 0.078, 0.118, 0.157, 0.222, 0.288 at a blowing ratio of 15, and $Sr = 0.034$, 0.102, 0.152, 0.203, 0.288, 0.372 at a blowing ratio of 10.

A constant fuel flow rate of 0.03 l/s and also a constant atomization airflow rate of 0.5 l/s are used. The remaining flow rates are primary combustion air and side air-jet flow rates of 11.8 and 10.3 l/s, respectively, for the blowing ratio of 15, and 14.2 and 8.0 l/s, respectively, for the blowing ratio of 10. At these flow rates, the jet Reynolds number $Re_{\text{jet}}[Re_{\text{jet}} = u_{\text{jet}}L/v$, where $L = \left(m_{\text{jet}}u_{\text{jet}}/\rho U_\infty^2\right)^{1/2}$ as suggested by

Broadwell and Breidenthal (1984)] is 2.9×10^5 for $R = 15$, and is 1.5×10^5 for $R = 10$. Corresponding crossflow (mainstream) Reynolds numbers ($Re_\infty = U_\infty D/v$) for these cases are 3×10^3 and 3.5×10^3 for $R = 15$ and $R = 10$, respectively. Blomeyer et al. (1999) report that the mixing process is to be minimally affected by mainstream Reynolds number and by mainstream turbulence intensity.

As briefly discussed in the literature survey, to establish a baseline to the degree of mixedness of the unforced jets with the mainstream, Holdeman (1993) used an empirical self-similarity parameter that he denoted as C. He recommended values of about 2.5 to be optimal. In the present study, the C values are considerably higher (19 and 12 for $R = 15$ and 10, respectively). However, Holdeman's study is based on nonreacting, nonswirling flows in a cylindrical tube. The present flow field is considerably more complex, and therefore the optimal parameters recommended by Holdeman do not necessarily apply here. In particular, higher blowing and momentum flux ratios were necessary in the present study (compared to those recommended by Holdeman), and these contribute to the higher C values. The emphasis was put on high momentum flux ratios and high mass flow additions due to the considerations related to (rich-burn/quick-quench/lean-burn (RQL) combustors because these high ratios are quite often used in RQL systems (Blomeyer et al., 1996). RQL combustion finds a wide spectrum of applications for itself, from power generation systems to commercial jetliners. It is well known that the rapid mixing in the Q section of these combustors yields reduced NO_x values. One of the key motivations for forced mass flow addition is to complete this mixing in a minimum possible downstream distance to reduce the overall combustor length.

Temperature Profiles

Due to the very low Mach number of the main flow, the temperatures measured by the thermocouples can essentially be interpreted as stagnation temperatures. Temperature data is presented only in the range $0.3 \leq z/D \leq 1.1$ where the jet-air mixing primarily takes place. However, it should be noted that combustion continues to take place farther downstream, and at the exit of the combustor ($z/D = 4$), the mean stack temperatures for the modulated and unmodulated cases are expected to be the same from first-law analysis, provided that same amount of fuel burns during the entire length.

Figures 7*a* and 7*b* show temperature contours at different elevations for blowing ratios of 15 and 10, respectively. These contours are shown only for one quadrant between two side air jets. Note that side air jets are introduced at $z/D = 0.2$, and the axial locations shown in Figure 7 are all downstream of the side air-jet injection. At $z/D = 0.3$ (the elevation closest to the side air-jet injection), the signature of unheated side air jet introduced into the heated stream is clearly visible (low-temperature region). The flame is partly quenched along the jet trajectory due to high strain rates and since the local equivalence ratio ϕ falls below the lean extinction limit of 0.5 (Westbrook et al., 1984). In the unforced case ($Sr = 0$), the jet can be said to be mostly concentrated around the periphery of the flame where a large cold region is evidently seen. Therefore, the jet penetration and the mixing around the jet periphery is quite poor. However, as the external forcing is introduced, the distance that the jet penetrates along its axis toward the flame is significantly increased. Significantly enhanced jet penetrations are observed at $Sr = 0.118$ and 0.222 for $R = 15$. Note that the two Sr values where the strongest penetration is observed are related to each other by a factor of 2, and potentially $Sr = 0.118$ is close to a subharmonic of $Sr = 0.222$. The strong jet penetration at $Sr = 0.222$ is in close agreement with the data of Vermeulen and Yu (1985), where they report a Sr of 0.250 as an optimal value for jet penetration. It is worth mentioning that Vermuelen and Yu (1985) obtained this optimal value while jets were discharged into a quiescent ambient not involving a swirling cross-flow. Other researchers (Karagozian et al., 2002; Narayanan et al., 2001) report similar optimal Strouhal numbers in the presence of nonswirling crossflows. Although it is known that swirl number greatly alters the baseline mixing condition, this evidence suggests that optimal Strouhal number and degree of mixing enhancement relative to the baseline condition (e.g., percentage PF reduction) with forcing may not be a strong function of swirl number.

As the jet at $R = 15$ is seen to penetrate deep into the flame regions at Strouhal numbers between 0.118 and 0.288, higher temperatures are observed downstream for these cases, compared to all other cases studied ($Sr = 0$, 0.026, 0.078). This is linked directly to the mixing enhancement and higher volumetric heat release induced by the jet modulation. Although local enhancements in temperatures as large as 300°C can be observed, the average enhancements appear to be more in the range 50–100°C.

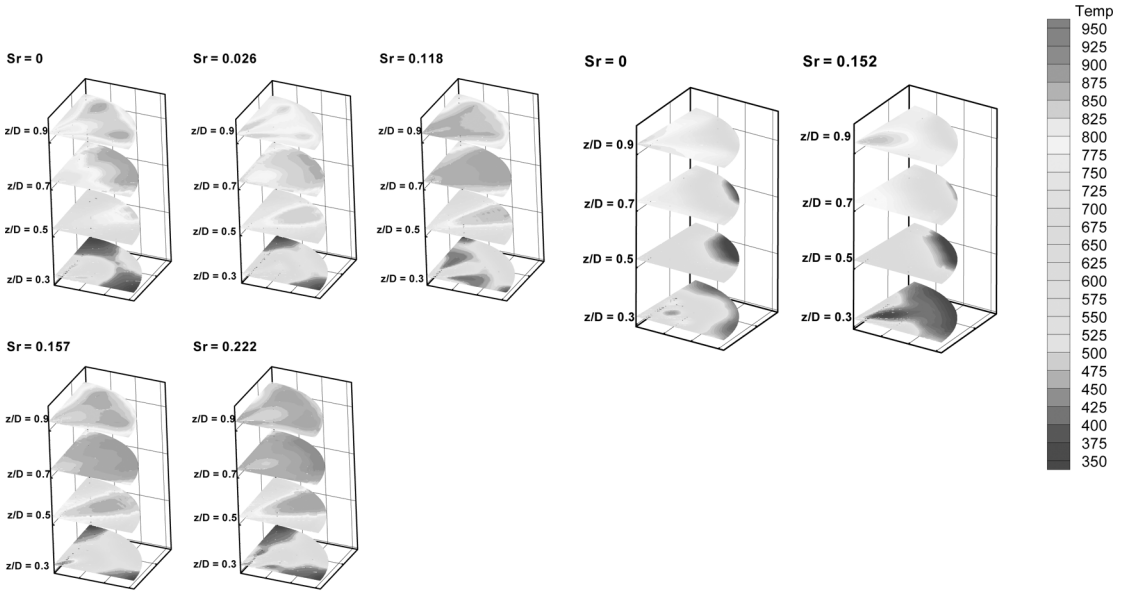

a. R=15 b. R=10

Figure 7. Three-dimensional temperature contours (temperatures in °C). (See Color Plate 1 at the end of this issue).

In comparing the baseline unmodulated case ($Sr = 0$) with the modulated cases, it is clear that the uniformity in the temperature distribution is enhanced both radially as well as circumferentially with forcing. At $z/D = 0.7$, for example, the baseline case shows significant radial variations in temperature with a cool inner core and a hot outer region where most of the burning takes place. With modulation and the associated enhanced mixing of the vaporized fuel and air, the radial distributions are relatively uniform. Thus, forcing frequency influences not only the magnitude but also the uniformity. However, the range of frequencies where the maximum heat release occurs ($Sr = 0.118$–0.222) does not correspond to the Sr value (0.026) with the most uniform distributions. More discussion on this issue is provided later in the section on pattern factors. At a blowing ratio of 10 (see Figure 7*b*), the effect of forcing is considerably reduced. This is associated with reduced jet penetration and a smaller spatial region of influence. At $Sr = 0.152$, the beneficial effects of modulation (higher temperature and volumetric heat release) are more apparent at locations further downstream of $z/D = 0.7$ and 0.9.

Figure 8 shows the radial distributions of temperature at different axial locations and one circumferential location ($\theta = 36^\circ$) corresponding to the side-jet injection location. Note that the radial temperature distribution at a fixed azimuthal location is only representative of a local effect. For $R = 15$, at $z/D = 0.56$, 0.81, and 1.08, higher temperatures are obtained with forcing with differences of the order of 60–70°C. Highest temperatures are generally obtained for $Sr = 0.222$, while at $Sr = 0.118$ (subharmonic) the temperature levels are comparably high but the distributions appear flatter. The flattest temperature distributions appear to correspond to the lowest modulation frequencies ($Sr = 0.026$). At $z/D = 0.30$, just downstream of the side air-jet injection location, the temperature distributions reflect the combined effects of localized flame quenching and enhanced mixing. For Strouhal numbers where the jet penetration is significant, the quenching effect is more apparent, as in $Sr = 0.118$. At the lowest frequency of $Sr = 0.026$, jet penetration is not as large, but the effect of the increased mixing is significant and provides the flattest temperature distribution. As noted earlier, the flattest temperature distributions at downstream locations also correspond to the lowest modulation frequency ($Sr = 0.026$).

For $R = 10$, the general observations are consistent with those observed at $R = 15$, except for differences in the levels of enhancement, and the relative roles of enhanced mixing versus localized quenching. At

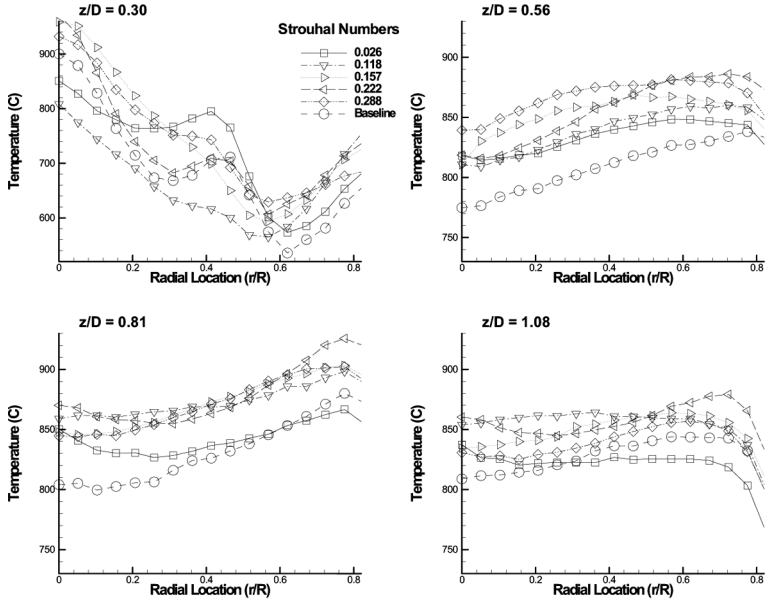

a. R=15, θ = 36°

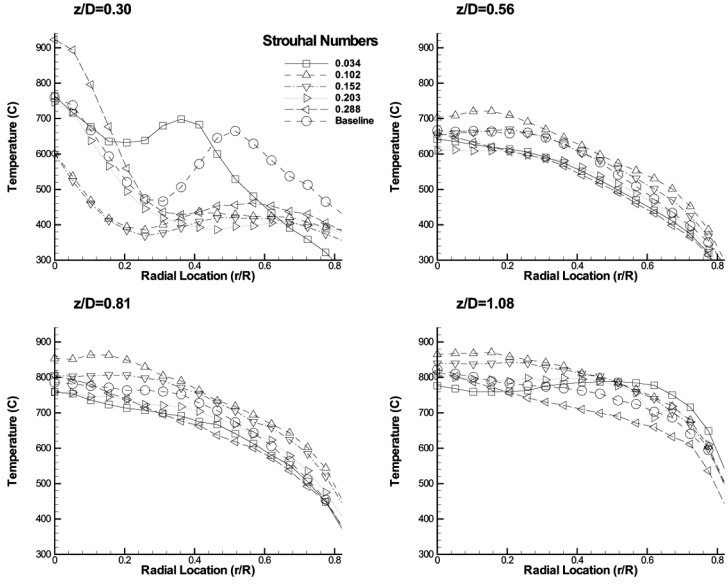

b. R=10, θ = 36°

Figure 8. Radial temperature profiles.

$z/D = 0.81$ and 1.08, modulation increases the temperatures at $Sr = 0.102$ and 0.152 due to the enhanced mixing effect, but at other modulation frequencies, this effect is not as strong, and temperatures even lower than the baseline can be seen due to localized quenching. The flattest temperature distributions are again achieved at the lowest Strouhal number considered for this blowing ratio.

Pattern Factors

The uniformity of the temperature profiles and, thus, air/fuel mixedness can be quantified by defining a PF as briefly mentioned in the introduction section. A planar PF is defined as follows in the present study:

$$PF(z) = \frac{T_{\max}(z) - \overline{T}(z)}{\overline{T}(z) - T_0} \tag{1}$$

where the radially weighted average temperature $\overline{T}(z)$ is the representative of the mean temperature in an (r, θ) plane. This is computed from the finite sum representation of the following equation,

$$\overline{T}(z) = \frac{\int\int T(r, \theta, z) r dr d\theta}{\int\int r dr d\theta} \tag{2}$$

Note that PFs are dimensionless numbers and can attain a minimum value of 0.0 in the limiting case where there is no spatial variation in the temperature data. Low PF values indicate a more uniform distribution with less variance in the temperature profile, whereas larger values signify stronger radial and circumferential thermal gradients.

Figure 9 shows the planar PFs plotted versus nondimensional height (z/D) from the dump plane for the baseline case and at different forcing frequencies. Note that the order of magnitude of these pattern factors is similar to those of the F-109 engine. This shall give necessary ground for the comparison of PF reduction. Regardless of the modulation frequency, PFs decrease with increasing elevation due to increased mixing. However, practical perspectives limit the length of combustors and are associated with unmixedness, but the goal of a combustion designer is the design of compact combustors with low PF in a minimum combustor length.

It is helpful to interpret Figure 9 with a perspective of the observations made in Figures 7*a* and 7*b*, which show the detailed temperature

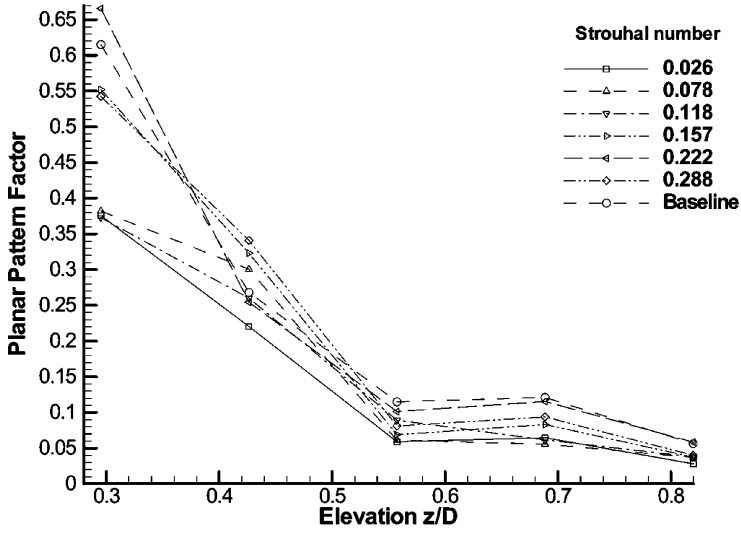

a. R=15

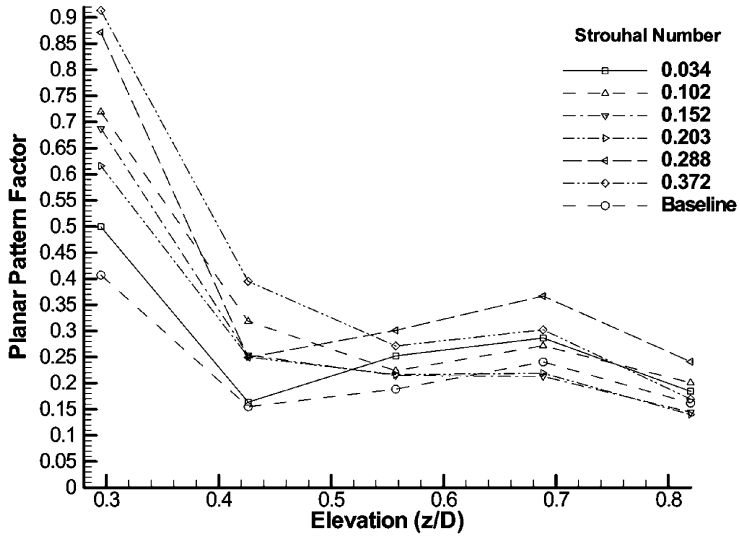

b. R=10

Figure 9. Planar pattern factors.

distributions inside the combustor. The most significant variation of the PF with different forcing frequencies occurs at elevations close to the dump plane. Farther downstream ($z/D > 0.7$), PF plots become gradually closer. In the primary combustion region ($z/D < 0.7$), the differences between the PFs can range from 0.1 to 0.4 at both blowing ratios. This is a significant effect and is clear evidence of the fact that the uniformity of the temperature field can be significantly altered with flow modulation, and that the modulation frequency can play an important role. Nonetheless, these plots also do indicate a trade-off between the performance merits; that is, the frequency showing the most favorable heat release characteristics does not possess the minimum pattern factor.

At $R = 15$, in general, modulation produces a decrease in PF over most of the combustor length, although over a short span (for z/D less than 0.4) there are frequencies showing higher PF than the baseline condition. The lowest forcing frequency ($Sr = 0.026$) clearly shows the lowest PF with a 0.25 absolute reduction (40% relative to baseline) in PF close to the dump plane and about a 0.07 absolute reduction (46% relative to baseline) relative to the unforced case reduction in PFs at around $z/D = 0.7$. Although absolute reduction decreases with increasing z/D, the order of magnitude of percentage reduction remains around 50% at all elevations.

For $R = 10$, PF results are not favorable and show an increase over the baseline case at nearly all frequencies. Thus, whereas temperatures are enhanced with modulation (Figure 8), the jet penetration and mixing are not strong enough to lead to a reduction in the PF. Rather, the localized quenching effect contributes to increasing the PF. Therefore, to utilize the side air jets to reduce PF, they should have sufficient momentum and control authority to enhance the mixing process.

Pressure and Heat Release Spectra

The combustion chamber is acoustically closed at one end and acoustically open at the other. Therefore, the dominant acoustic mode of the combustion chamber corresponds to a quarter-wave mode (Culick, 1976). This is seen in the Fourier spectra of pressure and heat release signals (see Figure 10) where there is a peak at the quarter-wave mode ($f_{1/4} = c/4H$) around 190 Hz. The other mode excited in the unforced case corresponds to a three-quarter-wave mode ($\lambda = 4/3H$). But, the amplitude of this excitation is rather weak and can be neglected. The

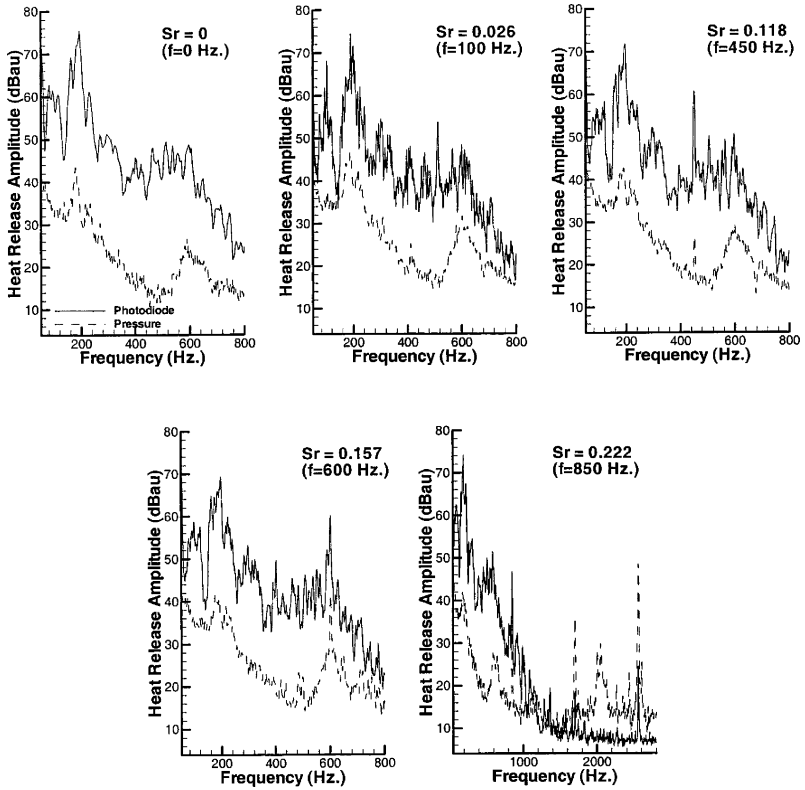

Figure 10. Pressure and heat release spectra at $R = 15$.

Strouhal number corresponding to the acoustic mode and the mainstream velocity ($Sr_\infty = f_{1/4}4H/U_\infty = 1/M_\infty$) is nearly 217, and is much higher than the Strouhal numbers associated with the side jet preferred mode. Therefore, in the present configuration, there is no interaction between the side air-jet frequencies and the acoustic frequencies, and the observed effects are primarily hydrodynamic. Another point is, if there were interaction between the jet mode and the dominant mode, one would expect energy transfer between these modes. However, the amplitude of the dominant mode remains invariant to the forcing frequency (see Figure 10), proving the absence of such an interaction.

In Figure 10, the spectral response of the pressure transducer and the CH photodiode are shown as a function of frequency. The CH photodiode is centered on the quartz window at a distance of 265 mm and has

a complete view of the main reaction zone, including the region where the side air jets are injected. The spectra clearly show both the acoustic mode of the main combustor as well as the forcing frequency. Open-loop forcing of the side air is not seen to alter the dominant mode of combustion. The added mode due to open-loop forcing at a constant frequency is responsible for the alteration of the temperature field. At most frequencies, amplitude of this mode is comparable to the amplitude of the dominant mode at the higher blowing ratio ($R = 15$). At the lower blowing ratio ($R = 10$), however, this amplitude is about 15–20 dB less than the amplitude of the dominant mode due to the lack of modulation strength delivered by the spinning valve. Therefore, at the lower blowing ratio, the control authority is not strong, and, as noted earlier in the temperature contours (see Figure 7*b*) and PF plots (see Figure 9), the beneficial effects at this lower blowing ratio are not as evident. Consequently, the amplitude of modulation plays a very important role in terms of establishing control authority over the flame.

The flame does not respond to pressure fluctuations roughly above 1.2 kHz. This is seen in Figure 9, where, for the 850 Hz forcing case, a strong second harmonic at 1.6 kHz in the pressure spectrum does not excite the corresponding heat release mode. Therefore, the response of the flame tapers off above a finite frequency. This effect is associated with a time lag between imposed velocity perturbations and heat release (Annaswamy et al., 1997).

Chemiluminescence Measurements

To spatially resolve the temporal heat release characteristics in the reaction zone, chemiluminescence measurements of the CH radical were performed. The CH radicals have been shown to be representative of the ethanol flame front (Bertran et al., 1998) and CH intensity correlates well with the local heat release for this type of fuel. An intensified Princeton Instruments PI-Max 512 T-18 G/III CCD camera with a 512×512 pixel resolution was utilized to acquire the images. The gate duration for the image acquisition was set to 0.10 μs.

A filter mounted on the camera lens is used to transmit the light at $\lambda = 390$ nm, which corresponds to the $B^2\Sigma^-$-$X^2\Pi(0,0)$ emission band of the CH radical (Garland et al., 1985), and to attenuate all other wavelength contributions. A Kistler 7061B piezoelectric pressure transducer mounted at the downstream end of the spinning valve provided the phase

information. Signal from the pressure transducer is fed into a DSPACE data acquisition board and the trigger signal (a transistor-transistor logic (TTL) pulse) is generated at the selected phase angle to trigger the camera. To resolve the complete cycle at each phase angle, a known time delay is added to the pressure signal. For the unmodulated case ($Sr = 0$), the phase locking is performed with respect to the dominant mode of combustion. At each triggering condition a sequence of 50 images was recorded. These sequences are then averaged to yield the corresponding mean intensity field.

The CH images presented in this section are taken at both of the blowing ratios of 15 and 10. Figure 11*a* shows the phase-averaged CH images at Strouhal numbers of 0 (steady side air jet) and 0.026 at 90° phase increments. The intensity images are presented on a pseudocolor scale with blue regions representing low CH intensities and red regions indicating high CH levels. In the images the signatures of the side air jets are clearly seen on both the left side and the right side. The conical flame is stretched

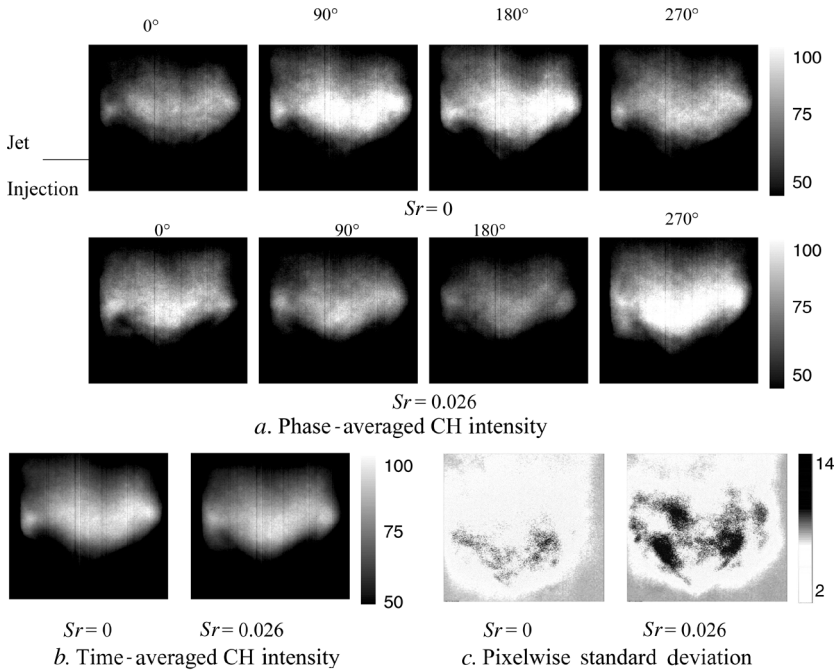

Figure 11. CH images at $R = 15$.

toward the side air jets, indicating their impact on the flame combustion. At both $Sr = 0$ and $Sr = 0.026$, the flame exhibits significant dynamics, with the dynamics at $Sr = 0.026$ representing intrinsic heat release variations associated with either the acoustics or the unsteady hydrodynamics and mixing. Since the reference trigger at $Sr = 0$ and $Sr = 0.026$ are different, the respective images in subfigures of Figure 11*a* cannot be directly compared, but it is evident that, with modulation, the heat release variations are altered both spatially and temporally.

Figure 11*b* shows the time-averaged CH-intensity distribution for the unmodulated ($Sr = 0$) and modulated ($Sr = 0.026$) cases at $R = 15$, whereas Figure 11*c* shows the corresponding standard deviation of the CH intensity. It is obvious from Figure 11*b* that, with modulation ($Sr = 0.026$), the time-averaged value of volumetric heat release within the reaction zone is enhanced by a significant amount. This is consistent with the three-dimensional temperature contour plots shown in Figure 7. However, Figure 11*c* suggests that temporal fluctuations in the heat release are stronger with forcing. This effect is due to larger velocity fluctuations associated with the side air jets.

CONCLUDING REMARKS

An experimental study is performed to explore the potential of modulating side air jets in a nonpremixed swirl-stabilized spray combustor to enhance volumetric heat release (leading to more compact combustors) and to lower PF (leading to lower emissions and reduced combustor length). It is shown that, by modulating the side air jets, the uniformity of the temperature profiles and the magnitude and distributions of the heat release patterns can be beneficially impacted. However, these two performance merits (volumetric heat release and PF) do not show the same dependence on the modulation frequency. The highest enhancements in volumetric heat release occur at frequencies close to the fundamental and subharmonic modes of the side air jets (*Sr* of approximately 0.22 and 0.11, respectively, for $R = 15$). These modes are associated with the greatest jet penetration. The lowest PF was observed at the lowest modulation frequency ($Sr = 0.026$ for $R = 15$) with percentage reductions in PF ranging from nearly 40% close to the dump plane to about 50% for $z/D > 0.7$. However, the absolute value of this reduction decreases monotonically with increasing z/D value due to increasing mixedness with increasing downstream length. At a lower blowing ratio

($R = 10$), the beneficial impacts of modulation were only observed in the volumetric heat release at select frequencies and indicated the importance of the air-jet momentum as an important control parameter. To have a significant effect, the forcing must impose pressure fluctuations that are at least as strong as the ones coming from the dominant acoustic modes of combustion. Nevertheless, typical PF reductions obtained with open-loop forcing are larger than the best enhancement (37%) obtained by passive means for the F-109 combustor.

The success in the results obtained so far with open-loop control via side air-jet modulation points to the potential of a closed-loop control strategy for optimizing PFs, volumetric heat release, and emissions. In the literature, simple feedforward multilayer-perceptron neural network (NN) architectures are shown to mimic the combustion output and track a desired PF input by controlling the dilution airflow rate (McManus and Lo, 1995). As a more advanced remedy for the current problem, the behavior of the plant at a multitude of load conditions can be construed as a feedback dynamic neural network, for system identification purposes, and genetic algorithms can be utilized to determine the optimum forcing conditions including the optimum forcing waveform (e.g., a periodic function identified by its Fourier coefficients). Such closed-loop strategies will be explored in the future.

NOMENCLATURE

a	offset between two parallel jet axis
C	Holdeman parameter, $=(S/D/2)\sqrt{J}$
c	speed of sound, $=\sqrt{\gamma RT}$
D	combustor diameter
d	jet exit diameter
f	frequency
F/A	fuel-to-air ratio
H	combustor height
J	jet-to-main flow momentum flux ratio
L	length scale
M	Mach number, $=U/c$
$\dot{m}$	mass flow rate
n	number of jet injection holes
PF	pattern factor, $=(T_{\max} - T_0)/(\bar{T} - T_0)$

R	blowing ratio, $u_{\text{jet}}/U_{\infty}$
r	radial position
Re	Reynolds number, $=uL_c/\nu$
S	circumferential spacing between orifice centers, $\pi(D/\sqrt{2})/n$
Sr	Strouhal number, $=fL_c/U$
Sw	swirl number
T	temperature
u	velocity
z	elevation measured from the dump plane

Greek Symbols

γ	specific heat ratio
θ	azimuthal position
λ	wavelength
ν	kinematic viscosity
ρ	density
ϕ	equivalence ratio, $=\frac{(F/A)_{\text{actual}}}{(F/A)_{\text{stochiometric}}}$

Subscripts

c	characteristic
max	maximum
o	inlet
jet	dilution jet
∞	main flow
1/4	quarter-wave mode
3/4	three-quarter wave mode
*	excited state

Superscript

–	average

REFERENCES

Alder, M.J., Tseng, L.K., Laurendeau, N.M., and Gore, J.P. (2000) Effects of partial premixing on NO_x emission indices of soot-containing flames. *Combust. Sci. Technol.*, **152**, 167–178.

Annaswamy, A.M., Fleifil, M., Hathout, J.P., and Ghoniem, A.F. (1997) Impact of linear coupling on the design of active controllers for thermoacoustic instability. *Combust. Sci. Technol.*, **128**, 131–180.

Beer, J.M. and Chigier, N.A. (1972) Combustion Aerodynamics, Applied Science Publishers, London.

Bertran, C.A., Marques, C.S.T., and Benvenutti, L.H. (1998) Mapping of luminescent species in a flame front. *Combust. Sci. Technol.*, **139**, 1–13.

Blomeyer, M., Krautkremer, B., and Hennecke, D.K. (1996) Optimum Mixing for a Two-Sided Injection from Opposing Rows of Staggered Jets into a Confined Crossflow. *Proceedings of the 1996 International Gas Turbine and Aeroengine Congress & Exhibition*, Birmingham, ASME paper 96-GT-453.

Blomeyer, M., Krautkremer, B., Hennecke, D.K., and Doerr, T. (1999) Mixing zone optimization of a rich-burn/quick-mix/lean-burn combustor. *J. Propul. Power*, **15**, 288–295.

Blossey, P.N., Narayanan, S., and Bewley, T.R. (2001) Dynamics and Control of Jets in Crossflow Direct Numerical Simulations & Experiments. *Proceedings of International Union of Theoretical and Applied Mechanics (IUTAM) Symposium on Turbulent Mixing and Combustion*, Kingston, Ontario, Canada.

Broadwell, J.E. and Breidenthal, R.E. (1984) Structure and mixing of a traverse jet in incompressible flow. *J. Fluid Mech.*, **148**, 405–412.

Cho, S.K., Yoo, J.Y., and Choi, H. (1998) Vortex pairing in an axisymmetric jet using two-frequency acoustic forcing at low to moderate Strouhal numbers. *Exp. Fluids*, **25**, 305–315.

Cortolezzi, L. and Karagozian, A.R. (2001) On the formation of counter-rotating vortex pair in traverse jets. *J. Fluid. Mech.*, **446**, 347–446.

Crocker, D.S., Smith, C.E., and Myers, G.D. (1994) Pattern Factor Reduction in a Reverse Flow Gas Turbine Combustor Using Angled Dilution Jets. *Proceedings of the International Gas Turbine and Aeroengine Congress and Exposition*, Hague, ASME paper 94-GT-406.

Culick, F.E.C. (1976) Non-linear behavior of acoustic waves in combustion chambers. *Acta Astronaut.*, **3**, 715–734.

Garland, N.L. and Crosley, D.R. (1985) Energy transfer processes in CH $A^2\Delta$ and $B^2\Sigma^-$ in an atmospheric pressure flame. *Appl. Opt.*, **24**, 4229–4237.

Holdeman, J.D. (1993) Mixing of multiple jets with a confined subsonic crossflow. *Prog. Energy Combust. Sci.*, **19**, 31–70.

Holdeman, J.D., Liscinsky, D.S., Samuelson, G.S., Oechsle, V.L., and Smith, C.E. (1996) *Mixing Of Multiple Jets with a Confined Subsonic Crossflow in a Cylindrical Duct*. ASME paper 96-GT-482.

Johari, H., Pacheco-Tougas, M., and Hermanson, J.C. (1999) Penetration and mixing of fully modulated turbulent jets in crossflow. *AIAA J.*, **37**, 842–850.

Karagozian, A.R., M'Closkey, R.T., King, J.M., and Cortelezzi, L. (2002) The actively controlled jet in crossflow. *J. Fluid Mech.*, **452**, 325–335.

Lilley, D.G. (2002) Jet injection into swirling crossflow for improved mixing and combustion. *Proceedings of the 2002 International Joint Power Generation Conference*, Phoenix, Arizona, USA, 881–888.

McManus, K. and Lo, E. (1995) Closed-loop system for control of combustor pattern factor. *Proceedings of the 1995 IEEE Conference on Control Applications*, Albany, 699–704.

Narayanan, S., Barooah, P., and Cohen, J.M. (2002) Experimental Study of the Coherent Structure Dynamics & Control of an Isolated Jet in Cross Flow. *40th Aerospace Sciences Meeting and Exhibit*, Reno, NV.

O'Donnell, M. (2001) Spray Combustion Laser Diagnostics and Combustion Control via Air Flow Fluctuations. Louisiana State University, Baton Rouge, LA.

Roy, G. (1998) Propulsion Combustion: Fuels to Emissions, Taylor & Francis, Bristol.

Vermeulen, P.J. and Yu, W.K. (1985) *An Experimental Study of Mixing by an Acoustically Pulsed Axisymmettrical Air Jet*. ASME paper 85-GT-49.

Vermeulen, P.J., Odgers, J., and Ramesh, V. (1982) *Acoustic Control of Dilution-Air Mixing in a Gas Turbine Combustor.* ASME paper 82-GT-35.

Vermeulen, P.J., Ramesh, V., and Yu, W.K. (1986) Measurements of entrainment by acoustically pulsed axisymmetric air jets. *J. Eng. Gas Turbine Power*, **108**, 479–484.

Westbrook, C.K. and Dryer, F.L. (1984) Chemical kinetic modeling of hydrocarbon combustion. *Prog. Energy Combust. Sci.*, **10**, 1–57.